Available online at www.sciencedirect.com
ScienceDirect
Journal of Solid State Chemistry 180 (2007) 2517–2524
JOURNAL OF SOLID STATE CHEMISTRY
www.elsevier.com/locate/jssc

Characterization of $Bi_5Nb_3O_{15}$ by refinement of neutron diffraction pattern, acid treatment and reaction of the acid-treated product with *n*-alkylamines

Seiichi Tahara[a], Akira Shimada[a], Nobuhiro Kumada[b], Yoshiyuki Sugahara[a,*]

[a]*Department of Applied Chemistry, School of Science and Engineering, Waseda University, 3-4-1, Ohkubo, Shinjuku-ku, Tokyo 169-8555, Japan*
[b]*Department of Research Interdisciplinary Graduate School of Medicine and Engineering, University of Yamanashi, Miyamae-cho 7, Kofu 400-8511, Japan*

Received 20 November 2006; received in revised form 7 May 2007; accepted 22 May 2007
Available online 25 May 2007

Abstract

The structure of $Bi_5Nb_3O_{15}$ was investigated by refinement of the powder neutron diffraction pattern as well as by structural change through acid treatment and subsequent treatments of an acid-treated product with *n*-alkylamines. Rietveld refinement suggests that $Bi_5Nb_3O_{15}$ adopts a mixed-layer Aurivillius-related phase structure, $[Bi_2O_2]+[NbO_4]+[Bi_2O_2]+[BiNb_2O_7]$ [*Pnc*2 (space group No. 30)] with $a = 2.1011(4)$, $b = 0.5473(1)$ and $c = 0.5463(1)$ nm. After the acid treatment of $Bi_5Nb_3O_{15}$ with 3 mol/L HCl, a new reflection (at 2.25 nm after drying at room temperature or at 1.89 nm after drying at 120 °C) appeared in the X-ray diffraction (XRD) pattern in addition to the reflections due to $Bi_5Nb_3O_{15}$. Upon acid treatment, a part of the Bi ions were lost and essentially no Nb ions were dissolved during acid treatment to give a Bi/Nb molar ratio of 1.4. The TG curves of the acid-treated product showed mass loss (ca. 4 mass%) in the range of 300–600 °C. It was also demonstrated that the particle shapes did not change upon acid treatment. The reaction of the acid-treated product (after drying at room temperature) with *n*-alkylamines led to a shift of the newly appearing reflection to a lower angle, and the *d*-value of the low-angle reflection increased linearly in accordance with the increment of the number of carbon atoms in *n*-alkylamines. These results indicate that the $[Bi_2O_2]$ sheet in $Bi_5Nb_3O_{15}$ was partially leached by acid treatment to form a layered compound $H_4BiNb_3O_{11}\cdot xH_2O$, capable of accommodating *n*-alkylamines in the interlayer space, and its anhydrous form, $H_4BiNb_3O_{11}$, upon drying. Based on the variation in the interlayer distance upon intercalation of *n*-alkylamines into the acid-treated product, the structure of the acid-treated product can be suggested to comprise alternately stacked protonated $[BiNb_2O_7]$ and $[NbO_4]$ sheets, a result consistent with the Rietveld refinement of $Bi_5Nb_3O_{15}$.

Keywords: Aurivillius phase; Neutron diffraction; Crystal structure; Layered perovskite; Intergrowth; Acid treatment; Intercalation; Ion exchange

1. Introduction

Layered perovskites consist of stacked nanosheets possessing (1 0 0)-terminated perovskite-like slabs $[A_{m-1}B_mO_{3m+1}]$ or (1 1 0)-terminated perovskite-like slabs $[A_mB_mO_{3m+2}]$ (*m*: thickness of the perovskite-like slabs). Among these, ion-exchangeable layered perovskites possess the exchangeable interlayer cation, M, between the (1 0 0)-terminated perovskite-like slabs and are expressed by the general formula $M_x[A_{m-1}B_mO_{3m+1}]$ [1]. They are categorized into two phases according to the amount of the interlayer cation per $[A_{m-1}B_mO_{3m+1}]$: Dion–Jacobson phases, $M[A_{m-1}B_mO_{3m+1}]$ ($x = 1$) [2,3], and Ruddlesden–Popper phases, $M_2[A_{m-1}B_mO_{3m+1}]$ ($x = 2$) [4,5]. Acid treatment of these phases leads to formation of their protonated forms, $H_x[A_{m-1}B_mO_{3m+1}]$ [1,6,7].

Aurivillius phases, $Bi_2A_{m-1}B_mO_{3m+3}$, are layered perovskites with intergrowth structures that have been attracting attention as ferroelectric materials [8–10]. The structures of the perovskite-like slabs in Aurivillius phases are essentially the same as those in ion-exchangeable layered perovskites, and Aurivillius phases possess $[Bi_2O_2]$ sheets instead of interlayer cations between the

*Corresponding author. Fax: +81 3 5286 3204.
E-mail address: ys6546@waseda.jp (Y. Sugahara).

0022-4596/$ - see front matter © 2007 Elsevier Inc. All rights reserved.
doi:10.1016/j.jssc.2007.05.017

perovskite-like slabs. Some Aurivillius phases can therefore be converted into new protonated forms of ion-exchangeable layered perovskites through acid treatment via selective leaching of $[Bi_2O_2]$ sheets [11–18]. It has been reported that there are some disorders occurring between A-site ions and bismuth ions ($[Bi_2O_2]$ sheets should therefore be $[(Bi,A)_2O_2]$ [13,14]) and that selective leaching provides direct insights into these disorders. Selective leaching can therefore be employed for structural characterization of the Aurivillius phases.

Some layered compounds can accommodate organic compounds in the interlayer space to form intercalation compounds consisting of alternatively stacked inorganic nanosheets and layers of organic molecules (or ions). The protonated forms of ion-exchangeable layered perovskites (Dion–Jacobson phases and Ruddlesden–Popper phases) as well as those derived from Aurivillius phases via selective leaching have been reported to exhibit the intercalation behavior of *n*-alkylamines [1,3,12,14,19–24]. Intercalation of guest species into layered compounds generally leads to expansion of the interlayer distance with no change in the lateral dimension [25,26]. Such phenomena provide insights not only into the conformation of the alkylchains in the interlayer space but also into the structure of the inorganic nanosheets [25].

Known Aurivillius-related phases include mixed-layer structures consisting of $Bi_2A_{m-1}B_mO_{3m+3}$ and $Bi_2A_mB_{m+1}O_{3m+6}$; the intergrowth structure can be expressed as $[Bi_2O_2]+[A_{m-1}B_mO_{3m+1}]+[Bi_2O_2]+[A_mB_{m+1}O_{3m+4}]$ [27–30]. Some mixed-layer Aurivillius-related phases have been characterized by X-ray diffraction (XRD) analysis and transmission electron microscopy (TEM) [28,31–33]. The bismuth niobate $Bi_5Nb_3O_{15}$ exhibits excellent ferroelectric, photocatalytic and optoelectric properties [29,30]. Its structure was proposed based on TEM observation to be a mixed-layer Aurivillius-related phase that can be expressed as $[Bi_2O_2]+[NbO_4]+[Bi_2O_2]+[BiNb_2O_7]$ ($m=1$, A = Bi) [31]. The structural refinement of $Bi_5Nb_3O_{15}$ as a mixed-layer Aurivillius phase was reported using the structure of $Bi_5TiNbWO_{15}$, but no details such as its atomic parameters and *R*-factors were provided because of the poor fitting [33]. The crystal structure of $Bi_5Nb_3O_{15}$ has therefore not been fully clarified to date.

Here, we report the structure of $Bi_5Nb_3O_{15}$ using Rietveld refinement of the powder neutron diffraction pattern, which can generally provide information concerning light elements such as oxygen atoms in transition metal oxides. In addition, acid treatment of $Bi_5Nb_3O_{15}$ and the reactions of the acid-treated product with *n*-alkylamines are reported; the original structure of $Bi_5Nb_3O_{15}$ is discussed and compared to the structural refinement based on the acid-treated product structure deduced from the relationship between the *d*-values of the products formed by the reaction of the acid-treated product with *n*-alkylamines.

2. Experimental section

Instrumentation: The XRD patterns were recorded on a Rigaku RINT-2500 diffractometer with monochromated Cu K_α radiation and a Rigaku RINT-1100 diffractometer with Mn-filtered Fe K_α radiation. The powder neutron diffraction pattern was obtained with HERMES, installed in the JRR-3M reactor at the Japan Atomic Energy Research Institute with a fixed wavelength of 0.181386 nm and a 2θ step size of 0.1° in the 2θ range from 7° and 157° (1500 data points). The neutron diffraction pattern was refined by a Rietveld refinement program, RIETAN 2000 [34]. The metal composition was determined by inductively coupled plasma emission spectrometry (ICP; Thermo Jarrel Ash, ICAP-574II) after dissolution with a HNO_3–H_2SO_4–HF mixture. The thermogravimetric (TG) curves were obtained with a Perkin-Elmer TGA7 in the range from room temperature to 900 °C (heating rate: 10 °C/min) under air flow. Infrared (IR) adsorption spectra were recorded on a JASCO FT/IR-460 Plus instrument with the KBr disk technique. Scanning electron microscopic (SEM) observation was conducted with a JEOL JSM-5600 microscope.

Preparation of $Bi_5Nb_3O_{15}$: $Bi_5Nb_3O_{15}$ was prepared by conventional solid-state reaction based on an earlier report [29]. A stoichiometric mixture of Bi_2O_3 and Nb_2O_5 was pressed to form pellets (ca. 80 kN). The pellets were heated at 800 °C for 2 h and at 1100 °C for 24 h.

Acid treatment of $Bi_5Nb_3O_{15}$ and reaction of the acid-treated product with n-alkylamines: For the acid treatment, 1 g of $Bi_5Nb_3O_{15}$ was dispersed in 200 mL of 3 mol/L hydrochloric acid at room temperature for 7 d. After centrifugation and washing with water, the product was dried at room temperature or 120 °C.

For the reaction with *n*-alkylamines, 0.1 g of the acid-treated product and 40 mL of an *n*-alkylamine–water mixture ($v/v=1$) (*n*-alkylamine: *n*-butylamine, *n*-hexylamine or *n*-octylamine) was sealed in a glass ampoule at 80 °C for 7 d. After centrifugation and washing with acetone, the product was dried at room temperature.

3. Results and discussion

3.1. Structural refinement of $Bi_5Nb_3O_{15}$

The XRD pattern of $Bi_5Nb_3O_{15}$ is shown in Fig. 1(a). This XRD pattern is consistent with the reported pattern and most of the reflections can be indexed with an orthorhombic cell. Weak reflections at $2\theta=10.9°$, 15.1° and 32.1° (marked with asterisks) could not, however, be indexed based on an orthorhombic cell. Although calcinations under different conditions were attempted to prepare single-phase $Bi_5Nb_3O_{15}$, these unindexed reflections always appeared.

Rietveld analysis using a neutron diffraction pattern was conducted based on the assumption that $Bi_5Nb_3O_{15}$ possesses a mixed-layer Aurivillius-related structure. Based

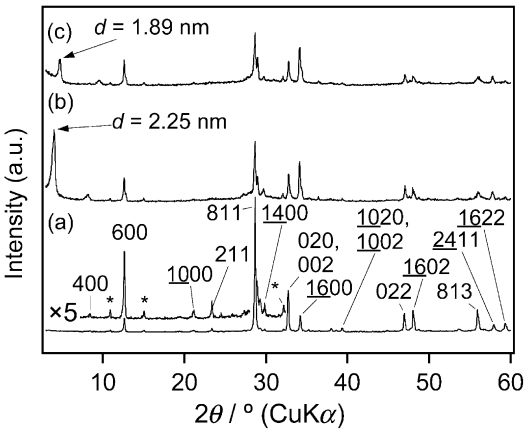

Fig. 1. The XRD patterns of (a) $Bi_5Nb_3O_{15}$, (b) the acid-treated product after drying at room temperature and (c) the acid-treated product after drying at 120 °C. Unindexed reflections are marked with asterisks.

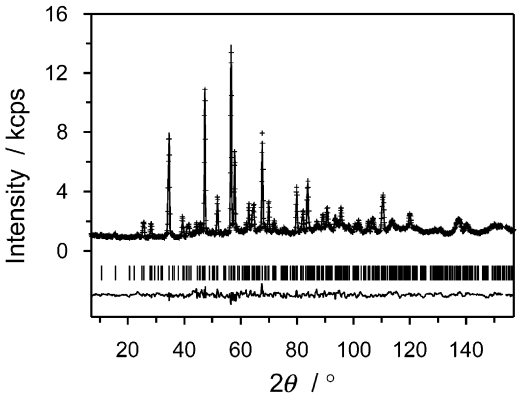

Fig. 2. Final Rietveld plot of $Bi_5Nb_3O_{15}$.

on an XRD pattern of $Bi_5Nb_3O_{15}$, the space group *Pnc*2 (space group No. 30) was selected to allow refinement.[1] Rietveld refinement of the neutron diffraction pattern led to reasonable *R*-factors, $R_{wp} = 7.16\%$, $R_p = 5.52\%$, $R_I = 5.50\%$, $R_F = 2.89\%$ and $S = 2.90$. The final Rietveld plot is shown in Fig. 2, and the final refined atomic parameters for the Rietveld refinement are listed in Table 1. The structure thus derived is illustrated in Fig. 3. The NbO_6 octahedra exhibit distortion and Nb–O distances are in the range of 0.181–0.231 nm, as indicated in Table 2.

Compared to the reported R_{wp} of $Bi_5TiNbWO_{15}$ (4.1%), the resultant R_{wp} (7.16%) is slightly high [33]. In addition, the bond valence sums approximately correspond to the theoretical values, but deviations from theoretical values are present for all the atoms (Table 2). These results might be caused by the fact that our sample was not a single-phase product. Thus, based on the structural refinements, we propose that $Bi_5Nb_3O_{15}$ possesses a mixed-layer Aurivillius-related phase structure, consisting of a $[Bi_2O_2]+[NbO_4]+[Bi_2O_2]+[BiNb_2O_7]$ stacking sequence, as illustrated in Fig. 3.

Table 1
The final refined atomic parameters for Rietveld neutron refinement of $Bi_5Nb_3O_{15}$, the space group *Pnc*2 ($Z = 2$) with $a = 2.1011(4)$, $b = 0.5473(1)$ and $c = 0.5463(1)$ nm

Atom	*x*	*y*	*z*	*U*
Bi(1)	0[a]	0.5[a]	0[a]	0.046(6)
Bi(2)	0.2442(5)	0.013(3)	0.481(7)	0.036(4)
Bi(3)	0.3675(5)	0.526(4)	0.484(4)	0.041(4)
Nb(1)	0.1074(4)	0.503(3)	0.480(6)	0.010(4)
Nb(2)	0.5[a]	0[a]	0.477(7)	0.006(5)
O(1)	0[a]	0.5[a]	0.393(7)	0.018(9)
O(2)	0.1949(8)	0.550(4)	0.426(8)	0.017(7)
O(3)	0.097(1)	0.187(6)	0.280(2)	0.06(1)
O(4)	0.0844(8)	0.754(5)	0.234(7)	0.017(4)
O(5)	0.413(1)	0.02(1)	0.395(1)	0.09(1)
O(6)	0.505(2)	0.218(5)	0.19(1)	0.06(1)
O(7)	0.305(1)	0.263(6)	0.229(9)	0.019(5)
O(8)	0.305(1)	0.748(6)	0.211(8)	0.011(5)

$R_{wp} = 7.16\%$, $R_p = 5.52\%$, $R_I = 5.50\%$, $R_F = 2.89\%$ and $S = 2.90$ for 422 reflections.
[a]Fixed values.

3.2. *Acid treatment of $Bi_5Nb_3O_{15}$ and reaction of the acid-treated product with n-alkylamines*

As described in the previous section, it seems likely that the structure of $Bi_5Nb_3O_{15}$ is a mixed-layer Aurivillius-related phase. Since the acid treatment of the Aurivillius-related structures is expected to provide further information for the crystal structures through selective leaching of Bi_2O_2 sheets [11], we conducted acid treatment of $Bi_5Nb_3O_{15}$ and characterized the resulting acid-treated product. The particle shapes of $Bi_5Nb_3O_{15}$ and the acid-treated product were investigated by SEM (Fig. 4(a) and (b)). Very similar plate-like particles can be observed in both the SEM images, demonstrating preservation of the particle shapes upon acid treatment. These results clearly contradict the occurrence of dissolution of $Bi_5Nb_3O_{15}$ in hydrochloric acid and subsequent precipitation.

The structure of the acid-treated product of $Bi_5Nb_3O_{15}$ was investigated by XRD analysis (Fig. 1(b) and (c)). The XRD pattern of the acid-treated product of $Bi_5Nb_3O_{15}$ shows the appearance of a new low-angle reflection at 2.25 nm in addition to the reflections due to $Bi_5Nb_3O_{15}$. In the XRD pattern of the product after drying at 120 °C, the reflection at 2.25 nm disappears and a new reflection is observed at 1.89 nm. The *d*-values of the low-angle reflections of $Bi_5Nb_3O_{15}$ (*a* lattice parameter) and the acid-treated product are listed in Table 3.

[1]For the structural refinement of $Bi_5Ti_{1.5}W_{1.5}O_{15}$ and $Bi_5TiNbWO_{15}$, both of which are isostructural with $Bi_5Nb_3O_{15}$, the refinement of the neutron diffraction pattern was attempted with another space group *Ima*2 (space group No. 46) [32,33]. In the structural refinement of the present results with the same space group, *Ima*2, however, negative isotropic atomic displacement parameters were obtained for some atomic sites. A similar result was reported for the structural refinement of $Bi_5Nb_3O_{15}$ with *Ima*2 [33].

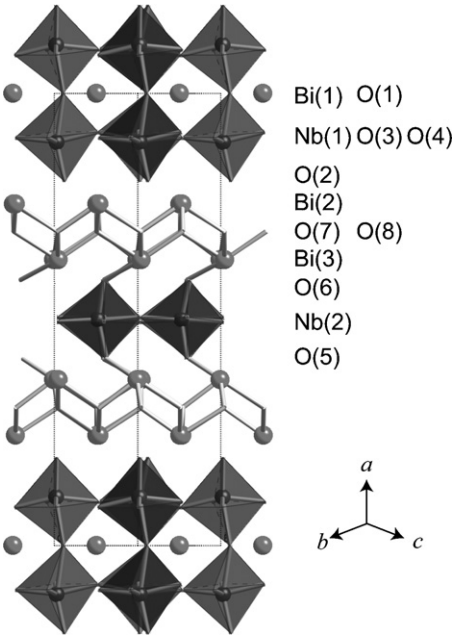

Fig. 3. Structure of $Bi_5Nb_3O_{15}$ derived from Rietveld structural refinement of the powder neutron diffraction pattern.

Table 2
Bond length of M–O bonds and bond valence sums of $Bi_5Nb_3O_{15}$ (M = Bi, Nb)

Bi(1)–O(1)	2.14(3)	Bi(2)–O(2)	2.67(3)	Bi(3)–O(5)	2.44(4)
Bi(1)–O(1)	2.798(9) × 2	Bi(2)–O(2)	2.75(3)	Bi(3)–O(5)	2.89(6)
Bi(1)–O(3)	2.59(3) × 2	Bi(2)–O(7)	2.23(4)	Bi(3)–O(5)	2.99(6)
Bi(1)–O(3)	3.08(3) × 2	Bi(2)–O(7)	2.33(4)	Bi(3)–O(6)	3.08(4)
Bi(1)–O(4)	2.59(3) × 2	Bi(2)–O(8)	2.30(4)	Bi(3)–O(7)	2.40(4)
Bi(1)–O(4)	2.66(3) × 2	Bi(2)–O(8)	2.44(3)	Bi(3)–O(7)	2.45(4)
				Bi(3)–O(8)	2.18(3)
				Bi(3)–O(8)	2.33(3)
ΣBi(1)	2.78	ΣBi(2)	2.57	ΣBi(3)	2.82
Nb(1)–O(1)	2.306(1)			Nb(2)–O(5)	2.00(2) × 2
Nb(1)–O(2)	1.88(2)				
Nb(1)–O(3)	1.95(5)			Nb(2)–O(6)	1.93(4) × 2
Nb(1)–O(3)	2.05(4)				
Nb(1)–O(4)	1.98(3)			Nb(2)–O(6)	1.98(5) × 2
Nb(1)–O(4)	1.98(3)				
ΣNb(1)	4.66			ΣNb(2)	5.46
ΣO(1)	2.09	ΣO(2)	1.59	ΣO(3)	2.08
ΣO(4)	2.39	ΣO(5)	1.87	ΣO(6)	2.16
ΣO(7)	2.21	ΣO(8)	2.47		

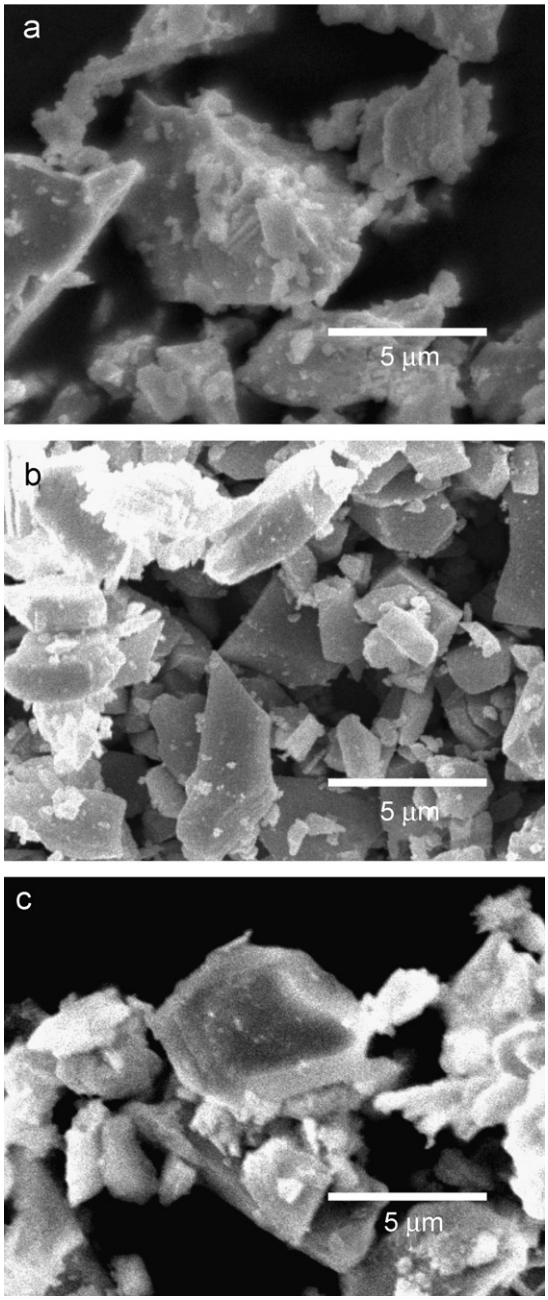

Fig. 4. The SEM images of (a) $Bi_5Nb_3O_{15}$, (b) the acid-treated product of $Bi_5Nb_3O_{15}$ and (c) the product of a reaction between the acid-treated product and *n*-butylamine.

Compositional analyses of $Bi_5Nb_3O_{15}$ and the acid-treated product by ICP demonstrate that the Bi/Nb molar ratio was drastically decreased from 5.0/3 to 1.4/3 (based on Nb = 3), as listed in Table S1 (Appendix A). The mass of $Bi_5Nb_3O_{15}$ after acid treatment was decreased from 1.0 to 0.51 g (51% yield), and the Nb content (34.8 mass%) in the acid-treated product therefore corresponds to 99% of Nb in original $Bi_5Nb_3O_{15}$ (17.8 mass%), indicating essentially no dissolution of Nb during acid treatment and selective dissolution of the Bi ions upon acid treatment. The TG curve of the acid-treated product after drying at 120 °C (Figure S1 in Appendix A) exhibits a gradual mass loss starting from room temperature with an abrupt change in mass (ca. 4 mass%) in the range of 300–600 °C, while no mass loss was observed up to 600 °C for original $Bi_5Nb_3O_{15}$.

Fig. 5 shows the XRD patterns (Fe K_α) of the products of the reactions between the acid-treated product and *n*-alkylamines. The XRD patterns show new low-angle reflections, shifting from 2.25 nm (dried at room temperature) to 2.78 nm (*n*-butylamine), 3.11 nm (*n*-hexylamine)

Table 3
d-Values of low-angle reflections after the acid treatment and the reaction of acid-treated product and *n*-alkylamines

Sample	*d*-Values of low-angle reflections (nm)
$Bi_5Nb_3O_{15}$	2.1011(4)[a]
Acid-treated product after drying at room temperature	2.25
Acid-treated product after drying at 120 °C	1.89
Product of the reaction of acid-treated product with *n*-butylamine	2.78
Product of the reaction of acid-treated product with *n*-hexylamine	3.11
Product of the reaction of acid-treated product with *n*-octylamine	3.30

[a] *a* lattice parameter.

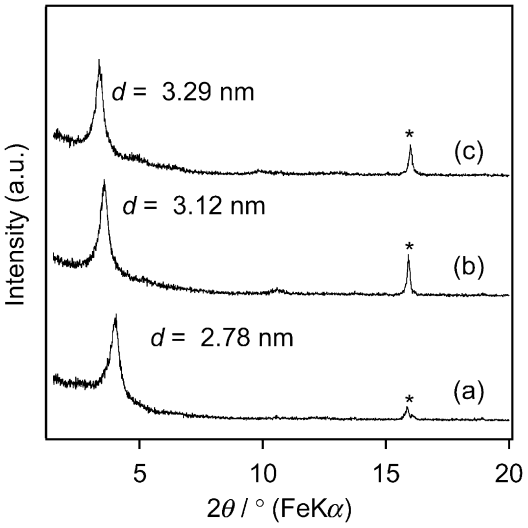

Fig. 5. The XRD patterns of the products of the reactions between the acid-treated product and (a) *n*-butylamine, (b) *n*-hexylamine and (c) *n*-octylamine. Reflections due to $Bi_5Nb_3O_{15}$ are marked with asterisks.

and 3.30 nm (*n*-octylamine). The *d*-values of the low-angle reflections of the products of the reactions of the acid-treated product with *n*-alkylamines are listed in Table 3 and the relationship between the number of carbon atoms, n_c, and the *d*-value of the low-angle reflection, *d*, is shown in Fig. 6. The relationship is linear and is expressed as $d = 0.13n_c + 2.30$ (nm). In addition, the IR spectra of the products (not shown) showed the presence of adsorption bands due to the *ν*(CH) mode at 2800–3000 cm^{-1}, the *δ*(NH) mode at 1600 cm^{-1} and the *ν*(CN) mode at 1150 cm^{-1} [35]. The SEM images also show no change in particle shapes during the reactions with *n*-alkylamines (Fig. 4(b) and (c)). These results suggest that the acid-treated product possesses a capability for uptake of *n*-alkylamines with an expansion along the stacking direction.

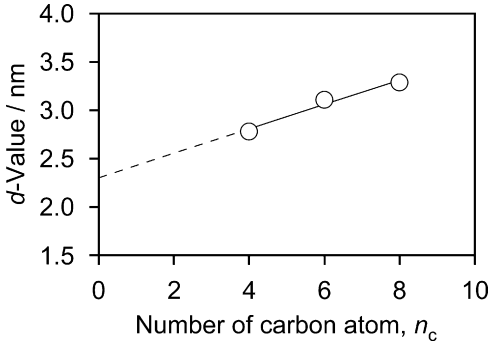

Fig. 6. The relationship between the number of carbon atoms, n_c, and the *d*-values of low-angle reflections of the products formed by the reactions of the acid-treated product with *n*-alkylamines.

3.3. Structure of the acid-treated product

Acid treatment of the Aurivillius phases, $Bi_2SrTa_2O_9$, $Bi_2A_2Nb_3O_{12}$ (A=Ca or Sr), $Bi_2CaNaTa_3O_{12}$ and $Bi_2W_2O_9$, led to the formation of protonated phases via selective leaching of $[(Bi,A)_2O_2]$ sheets. In these conversions, the following phenomena were observed: (1) the appearance of a new reflection at a higher angle appeared in the XRD pattern of the acid-treated product after drying at 120 °C, (2) selective dissolution of Bi, (3) the occurrence of mass loss of the TG curves of the acid-treated product after drying at 120 °C in the range from 200 to 600 °C and (4) preservation of the particle shapes [13,14,16,17]. In the present study, the following four phenomena are correspondingly observed: the appearance of a new reflection at a higher angle in the XRD pattern of the acid-treated product after drying 120 °C (1.89 nm), selective dissolution of Bi ions, mass loss of the TG curve of the acid-treated product after drying at 120 °C in the range from 300 to 600 °C and preservation of the particle shapes as revealed by SEM. The occurrence of mass loss of the TG curve suggests that protons are present in the acid-treated product. (So far we could not interpret the occurrence of gradual mass loss from room temperature, so that we tentatively attribute the mass loss in the temperature range of 300–600 °C, which is higher than the previously observed temperature range [13,14,16,17], to a loss of protons in the interlayer space as H_2O molecules.)

In addition, the acid-treated product exhibits a capability for uptake of *n*-alkylamines in accordance with acidity due to the presence of protons. A linear relationship is observed between the number of carbon atoms, n_c, and *d*-value of the low-angle reflection, *d*, and similar linear relationships were reported for the intercalation of *n*-alkylamines into various layered compounds [25,36], including protonated forms of the Dion–Jacobson phases [19]. The present results therefore suggest the formation of a new protonated layered compound, which can accommodate *n*-alkylamines in the interlayer space, via the selective leaching of $[Bi_2O_2]$ sheets.

According to the previous conversions [13,14,16,17], the present results can be interpreted based on the following

idealized reaction:

$$Bi_5Nb_3O_{15} \xrightarrow{HCl} H_4BiNb_3O_{11}. \quad (1)$$

In the XRD patterns, two low-angle reflections are observed at 2.25 and 1.85 nm depending on drying conditions, indicating the presence of two kinds of layered compounds. Thus, a layered compound with a repeating distance of 2.25 nm (obtained by drying at room temperature) is an $H_4BiNb_3O_{11}$ hydrated phase, $H_4BiNb_3O_{11} \cdot xH_2O$, and a layered compound with repeating distance of 1.89 nm is anhydrous phase, $H_4BiNb_3O_{11}$, which forms after drying at 120 °C.

In the present study, the resultant Bi/Nb molar ratio (1.4/3) is higher than the expected value (1/3), suggesting partial occurrence of selective leaching of $[Bi_2O_2]$ sheets. This result is consistent with the XRD results (Fig. 1), in which reflections due to $Bi_5Nb_3O_{15}$ are observed. We attempted the acid treatment of $Bi_5Nb_3O_{15}$ under different conditions (different types of acids, concentrations of hydrochloric acid, reaction time, temperatures, etc.) to obtain a single-phase product (with a Bi/Nb molar ratio of 1/3). When concentrated acid was used, $Bi_5Nb_3O_{15}$ was mostly dissolved in acid. Milder reaction conditions such as the use of low concentration of acid and fewer acid treatments led to the formation of products with the Bi/Nb molar ratios higher than 1.4/3, indicating that acid treatment was insufficient. Thus, we have so far been unable to obtain the single-phase product, but it should be noted that the acid-treated products with milder acid treatment (after drying at room temperature) possessed new low-angle reflections, whose *d*-values (2.25 nm) were the same as that observed for acid-treated product after drying at room temperature with a Bi/Nb molar ratio of 1.4/3 (corresponding to repeating distance of $H_4BiNb_3O_{11} \cdot xH_2O$). When the acid-treated products after drying at room temperature with different molar ratio of Bi/Nb were allowed to react with *n*-butylamine, the XRD patterns of all the products showed the appearance of a new reflection at 2.78 nm and the disappearance of the low-angle reflection due to $H_4BiNb_3O_{11} \cdot xH_2O$. These results indicate that acid treatment resulted in the formation of a layered compound, $H_4BiNb_3O_{11} \cdot xH_2O$, that can accommodate *n*-alkylamine irrespective of acid treatment conditions. We therefore conclude that the acid-treated products essentially consist of $H_4BiNb_3O_{11} \cdot xH_2O$ and unreacted $Bi_5Nb_3O_{15}$. Based on this interpretation, the Bi/Nb molar ratio (1.4/3) indicates that 90% of $Bi_5Nb_3O_{15}$ is converted into $H_4BiNb_3O_{11} \cdot xH_2O$.

For the linear relationship in Fig. 6, the intercept, 2.30 nm, could be regarded as a hypothetical *d*-value of the intercalation compound possessing NH_3 in the interlayer space. The difference in value between the intercept and the *d*-value of the acid-treated product after drying at 120 °C, Δd, is calculated as follows and is listed in Table 4:

$$\Delta d = [\text{intercept, } (A), \text{ 2.30 nm}] - [d\text{-value of acid-treated product after drying 120 °C, } (B), \text{ 1.89 nm}] = 0.41 \text{ nm}.$$

In a similar fashion, the Δd values for other protonated forms of ion-exchangeable layered perovskites are calculated based on the reported intercalation behavior of *n*-alkylamines (Table 3) [19,21]. These Δd values in previous reports can be compared with the diameter of the NH_4^+ ion, 0.29 nm [37,38], which should be similar to that of NH_3; the Δd values are nearly equal to or smaller than the diameter of the NH_4^+ ion. The Δd value in the present study (0.41 nm), which is much larger than the diameter of the NH_4^+ ion, therefore seems to suggest the presence of two NH_3 layers in the unit cell of the acid-treated product. Since the *d*-values of the lower-angle reflections of the acid-treated products (2.25 nm for the air-dried product and 1.89 nm for the product after drying at 120 °C) are nearly equal to the *a* lattice parameter (a=2.1011(4) nm) of $Bi_5Nb_3O_{15}$, the repeating distance along the stacking direction of the acid-treated products is assumed to correspond to one $[NbO_4]$ sheet and one $[BiNb_2O_7]$ sheet. If two $[Bi_2O_2]$ sheets in a unit cell of $Bi_5Nb_3O_{15}$ are leached by acid treatment to form a new layered compound possessing two interlayer spaces and these sheets stack with no displacement, one $[NbO_4]$ sheet and one $[BiNb_2O_7]$ sheet should be present in the repeating distance (Fig. 7). These considerations give us a $Bi_5Nb_3O_{15}$ structure possessing an $[NbO_4]$ sheet, a $[BiNb_2O_7]$ sheet and two $[Bi_2O_2]$ sheets in the unit cell, a model exhibiting excellent consistency with the aforementioned structure of

Table 4
The differences between the intercepts in the n_c–*d* relationships of the *n*-alkylamine intercalation compounds and the *d*-values of the protonated forms of ion-exchangeable layered perovskites

	Intercept (*A*) (nm)	*d*-Value of the acid-treated product (*B*) (nm)	Difference (*A*)−(*B*) (nm)
The present study	2.30	1.89	0.41
n-Alkylamine–$H_{1.8}Bi_{0.2}Sr_{0.8}Ta_2O_7$ intercalation compounds [21]	1.13	0.98	0.15
n-Alkylamine–$HCa_2Nb_3O_{10}$ intercalation compounds for n_c = 2–5 [19]	1.62	1.44	0.18
n-Alkylamine–$HCa_2Nb_3O_{10}$ intercalation compounds for n_c = 12–18 [19]	1.71	1.44	0.27

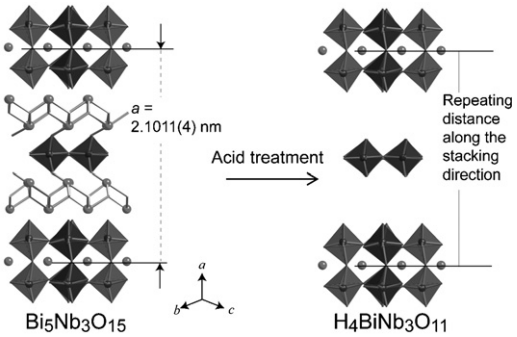

Fig. 7. Structural model of the acid-treated product.

$Bi_5Nb_3O_{15}$, which consists of a $[Bi_2O_2]+[NbO_4]+[Bi_2O_2]+[BiNb_2O_7]$ stacking sequence.

Taking the interpretation that acid-treated product possesses two interlayer spaces, a $[BiNb_2O_7]$ sheet and an $[NbO_4]$ sheet into account, a slope of the linear relationship per interlayer is estimated to be 0.065(=0.13/2) nm/carbon atom, and the slope is smaller than increment length of *all-trans* alkylchain per one carbon atom, 0.127 nm. Based on this value, two types of possible models can be proposed for intercalation compounds: (1) interdigitated monolayer arrangement of *n*-alkylchains with tilting angle 28° and (2) bilayer arrangement of *n*-alkylchains with tilting angle 15° [25]; we cannot further discuss which model is appropriate based on the present results.

4. Conclusions

We have demonstrated the characterization of $Bi_5Nb_3O_{15}$ by refinement of the powder neutron diffraction pattern, and the structure derived from the structural refinement is confirmed by acid treatment of $Bi_5Nb_3O_{15}$ and the reaction of the acid-treated product with *n*-alkylamines. $Bi_5Nb_3O_{15}$ seems to adopt a mixed-layer Aurivillius-related phase structure with the orthorhombic cell (a=2.1011(4), b=0.5473(1) and c=0.5463(1) nm and $Z=2$). Acid treatment of $Bi_5Nb_3O_{15}$ leads to partial leaching of the $[Bi_2O_2]$ sheets to form a new layered compound, $H_4BiNb_3O_{11}\cdot xH_2O$, possessing a capability for accommodation of *n*-alkylamines, and its anhydrous form, $H_4BiNb_3O_{11}$, upon drying. The intercalation behavior of *n*-alkylamines indicates the presence of two interlayer spaces, which are originally occupied by $[Bi_2O_2]$ sheets in the intergrowth structure of $Bi_5Nb_3O_{15}$, in $H_4BiNb_3O_{11}$ with a repeating distance (1.89 nm), a result consistent with the structural refinement of $Bi_5Nb_3O_{15}$. This study provides a detailed structural characterization of $Bi_5Nb_3O_{15}$, and the present structural characterization approach might be adaptable, moreover, to other intergrowth structures.

Acknowledgment

This work was financially supported in part by 21COE "Practical nano-chemistry" from the Ministry of Education, Culture, Sports, Science and Technology (MEXT), Japan.

Appendix A. Supplementary materials

Supplementary data associated with this article can be found in the online version at doi:10.1016/j.jssc.2007.05.017

References

[1] R.E. Schaak, T.E. Mallouk, Chem. Mater. 14 (2002) 1455–1471.
[2] M. Dion, M. Ganne, M. Tournoux, Mater. Res. Bull. 16 (1981) 1429–1435.
[3] A.J. Jacobson, J.W. Johnson, J.T. Lewandouski, Inorg. Chem. 24 (1985) 3727–3729.
[4] S.N. Ruddlesden, P. Popper, Acta Crystallogr. 10 (1957) 538–539.
[5] S.N. Ruddlesden, P. Popper, Acta Crystallogr. 11 (1958) 54–55.
[6] A.J. Jacobson, J.T. Lewandouski, J.W. Johnson, J. Less-Common Met. 116 (1986) 137–146.
[7] J. Gopalakrishnan, V. Bhat, Inorg. Chem. 26 (1987) 4299–4301.
[8] B. Aurivillius, Ark. Kemi 1 (1949) 463–480.
[9] B. Aurivillius, Ark. Kemi 1 (1949) 499–512.
[10] B. Aurivillius, Ark. Kemi 2 (1950) 519–527.
[11] S. Tahara, Y. Sugahara, Recent Res. Dev. Inorg. Chem. 4 (2004) 13–35.
[12] W. Sugimoto, M. Shirata, Y. Sugahara, K. Kuroda, J. Am. Chem. Soc. 121 (1999) 11601–11602.
[13] Y. Tsunoda, M. Shirata, W. Sugimoto, Z. Liu, O. Terasaki, K. Kuroda, Y. Sugahara, Inorg. Chem. 40 (2001) 5768–5771.
[14] W. Sugimoto, M. Shirata, K. Kuroda, Y. Sugahara, Chem. Mater. 14 (2002) 2946–2952.
[15] M. Shirata, Y. Tsunoda, W. Sugimoto, Y. Sugahara, Mater. Res. Soc. Symp. Proc. 658 (2001) GG.6.24.21–GG.26.24.25.
[16] M. Kudo, S. Tsuzuki, K. Katsumata, A. Yasumori, Y. Sugahara, Chem. Phys. Lett. 393 (2004) 12–16.
[17] M. Kudo, H. Ohkawa, W. Sugimoto, N. Kumada, Z. Liu, O. Terasaki, Y. Sugahara, Inorg. Chem. 42 (2003) 4479–4484.
[18] R.E. Schaak, T.E. Mallouk, Chem. Commun. (2002) 706–707.
[19] A.J. Jacobson, J.W. Johnson, J.T. Lewandouski, Mater. Res. Bull. 22 (1987) 45–51.
[20] J. Gopalakrishnan, V. Bhat, B. Raveau, Mater. Res. Bull. 22 (1987) 413–417.
[21] Y. Tsunoda, W. Sugimoto, Y. Sugahara, Chem. Mater. 15 (2003) 632–635.
[22] S. Tahara, T. Yamashita, G. Kajiwara, Y. Sugahara, Chem. Lett. 35 (2006) 1292–1293.
[23] Z.W. Tong, G.Z. Zhang, S. Takagi, T. Imai, H. Tachibana, H. Inoue, Chem. Lett. 34 (2005) 632–633.
[24] S. Tahara, T. Ichikawa, G. Kajiwara, Y. Sugahara, Chem. Mater. 19 (2007) 2352–2358.
[25] M.S. Whittingham, A.J. Jacobson (Eds.), Intercalation Chemistry, Academic Press, New York, 1982.
[26] S.M. Auerbach, K.A. Carrado, P.K. Dutta (Eds.), Handbook of Layered Materials, Marcel Dekker Inc., New York, 2004.
[27] R.J.D. Tilley, in: M.W. Robert, J.M. Thomas (Eds.), Chemical Physics of Solids and Their Surfaces, vol. 8, Specialist Periodic Report, The Royal Society of Chemistry, London, 1980.
[28] J. Gopalakrishnan, A. Ramanan, C.N.R. Rao, D.A. Jefferson, D.J. Smith, J. Solid State Chem. 55 (1984) 101–105.
[29] T. Takenaka, K. Komuro, K. Sakata, Jpn. J. Appl. Phys. Part. 1 (35) (1996) 5080–5083.
[30] K. Gurunathan, P. Maruthamuthu, J. Solid State Electrochem. 2 (1998) 176–180.

[31] W. Zhou, D.A. Jefferson, J.M. Thomas, in: A. Navrotsky, D.J. Weindner (Eds.), A Structure of Great Interest to Geophysics and Materials Science, vol. 45, American Geophysical Union, Washington, DC, 1989, pp. 113–117.
[32] J. Tellier, P. Boullay, N. Créon, D. Mercurio, Solid State Sci. 7 (2005) 1025–1034.
[33] A. Snedden, D.O. Charkin, V.A. Dolgikh, P. Lightfoot, J. Solid State Chem. 178 (2005) 180–184.
[34] F. Izumi, T. Ikeda, Mater. Sci. Forum 321–324 (2000) 198–203.
[35] H.F. Shurvell, in: J.M. Chalmers, P.R. Griffiths (Eds.), Handbook of Vibrational Spectroscopy, vol. 3, Wiley, Chichester, UK, 2002, pp. 1783–1816.
[36] G. Lagaly, Angew. Chem. Int. Ed. Engl. 15 (1976) 575–586.
[37] P.U. Oyari, O.Y. Samoilov, J. Struct. Chem. 12 (1971) 838–840.
[38] T. Akutagawa, T. Hasegawa, T. Nakamura, T. Inabe, J. Am. Chem. Soc. 124 (2002) 8903–8911.